Spectrally selective solar absorber with sharp and temperature dependent cut-off based on semiconductor nanowire arrays

Cite as: Appl. Phys. Lett. **110**, 201108 (2017); https://doi.org/10.1063/1.4983711
Submitted: 23 January 2017 . Accepted: 30 April 2017 . Published Online: 18 May 2017

Yang Wang, Lin Zhou, Qinghui Zheng, Hong Lu, Qiaoqiang Gan, Zongfu Yu, and Jia Zhu

Spectrally selective solar absorber with sharp and temperature dependent cut-off based on semiconductor nanowire arrays

Yang Wang,[1] Lin Zhou,[1] Qinghui Zheng,[1] Hong Lu,[1] Qiaoqiang Gan,[2] Zongfu Yu,[3] and Jia Zhu[1,a)]

[1]*National Laboratory of Solid State Microstructures, College of Engineering and Applied Sciences, and Collaborative Innovation Center of Advanced Microstructures, Nanjing University, Nanjing, 210093, China*
[2]*Department of Electrical Engineering, University at Buffalo, The State University of New York, Buffalo, New York 14260, USA*
[3]*Department of Electrical and Computer Engineering, University of Wisconsin Madison, Madison, Wisconsin 53706, USA*

(Received 23 January 2017; accepted 30 April 2017; published online 18 May 2017)

Spectrally selective absorbers (SSA) with high selectivity of absorption and sharp cut-off between high absorptivity and low emissivity are critical for efficient solar energy conversion. Here, we report the semiconductor nanowire enabled SSA with not only high absorption selectivity but also temperature dependent sharp absorption cut-off. By taking advantage of the temperature dependent bandgap of semiconductors, we systematically demonstrate that the absorption cut-off profile of the semiconductor-nanowire-based SSA can be flexibly tuned, which is quite different from most of the other SSA reported so far. As an example, silicon nanowire based selective absorbers are fabricated, with the measured absorption efficiency above (below) bandgap ~97% (15%) combined with an extremely sharp absorption cut-off (transition region ~200 nm), the sharpest SSA demonstrated so far. The demonstrated semiconductor-nanowire-based SSA can enable a high solar thermal efficiency of ≳86% under a wide range of operating conditions, which would be competitive candidates for the concentrated solar energy utilizations. *Published by AIP Publishing.*
[http://dx.doi.org/10.1063/1.4983711]

For a wide range of solar energy conversion systems, such as concentrating solar power,[1,2] solar thermochemical,[3] solar thermophotovoltaics,[4–6] and solar thermoelectric systems,[7] spectrally selective absorbers (SSA) are critical components due to their ability of suppressing radiation loss, particularly under high temperature or highly concentrated solar irradiance operation conditions.[8–10] Extensive efforts have been devoted to the design and fabrication of various SSA, such as ceramic-metal composites,[11–14] intrinsic semiconductor materials,[15–17] multilayer structures, and various nanophotonic structures.[18–24] While various SSA with high solar absorption and low infrared emission have been demonstrated, most of them are not favorable for high temperature operation because of not well defined absorption cut-off profile. As operating temperatures elevate, the energy loss due to the spectral overlap between the concentrated solar spectrum and the radiation spectrum becomes significant (Fig. 1), and a sharp cut-off between the high solar absorption band and the low infrared emission band is critical for efficient solar energy conversion, which has rarely been explored so far.

The optical performance of SSA is commonly determined by the ratio of the solar absorptivity and thermal emissivity, which dominates the thermal transfer efficiency (η) of SSA

$$\eta = \frac{C\int \alpha(\lambda)E_{solar}(\lambda)d\lambda - \int \alpha(\lambda)E_B(\lambda,T)d\lambda}{C\int E_{solar}(\lambda)d\lambda}, \quad (1)$$

where α is the absorptivity of SSA in thermal equilibrium, which is equal to the emissivity at each wavelength (λ) according to Kirchhoff's law. E_{solar} is the solar spectral irradiance, E_B is the blackbody spectral irradiance, and C is the solar concentration. To achieve efficient solar-thermal conversion, the ideal absorptivity profile of SSA should have a proper cut-off wavelength with respect to the operating conditions (temperature, optical concentration, etc.) as well as an optimized absorption edge with the step-function profile.[25] Here, we will show the significance of the absorption cut-off profile quantitatively.

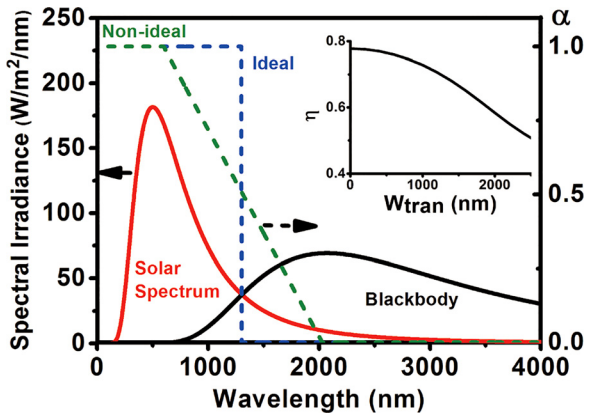

FIG. 1. Spectra overlap of blackbody at 1400 K (black solid line) and solar irradiation (red solid line). Absorptivity of the absorber (α_h=1, α_l=0) with W_{tran} of 0 (blue dash, ideal cut-off) and 1500 nm (green dash, non-ideal cut-off). The inset shows the dependence of solar thermal transfer efficiency (η) on the absorption transition width (W_{tran}).

a)jiazhu@nju.edu.cn

Without loss of generality, the degree of absorption cut-off can be quantified as the bandwidth of the transition region (W_{tran}) between the high absorption (α_h) band and the low emission (α_l) band, i.e.

$$W_{tran} = \lambda_{\min}(\alpha_l) - \lambda_{\max}(\alpha_h), \tag{2}$$

where α_h and α_l are the upper and lower absorptivity of SSA, respectively. Therefore, smaller W_{tran} represents sharper absorption cut-off and higher selectivity. Taking a selective absorber that works at 1400 K under 100-sun irradiation as an example (Fig. 1), because of the significant spectrum overlap between the solar irradiation and black body radiation, the solar thermal efficiency shows a strong dependence on W_{tran}. As W_{tran} increases from 0 to 2000 nm (Fig. 1, inset), thermal transfer efficiency decreases rapidly from 77% to 58% provided that the absorber has an ideal upper and lower absorptivity ($\alpha_h = 1$, $\alpha_l = 0$, dashed line in Fig. 1). It means that sharp absorption cut-off is critical for efficient solar thermal conversion. However, most of the previous studies have mainly focused on the absorption selectivity instead of the absorption cut-off (supplementary material, Table S1 of Part I). In addition, most of the spectrum selective absorbers only work efficiently under limited working conditions because of their fixed cut-off wavelength. In this letter, based on systematical study on the absorption cut-off as well as temperature dependent semiconductor properties, we demonstrate that the semiconductor nanowires enabled SSA with the sharpest absorption cut-off that are favorable for a wide range of operating conditions.

It is known that bulk semiconductor materials are not ideal SSA for at least three reasons. (1) Due to the large refractive index mismatch between the semiconductor and air, there is a significant reflection loss at the surface. (2) Sub-bandgap absorption of semiconductors due to activated impurities and free carrier absorption would greatly increase the absorption below the bandgap and finally deteriorate the absorption selectivity. (3) For an indirect bandgap semiconductor (such as silicon), the absorption close to the bandgap is usually inefficient because of the momentum mismatch and therein ultralow interband transition probability.

In the past few decades, nanostructures and anti-reflection coatings have been employed to reduce the optical reflection and thus enhance absorption.[23,24,26–29] Recently, Bermel *et al.*[6] theoretically discussed the performance of the smooth silicon absorber at 1000 K based on a simplified model, in which only the interband absorption was considered while the sub-bandgap absorption was ignored. In the current study, sub-bandgap absorption because of free carrier absorption at elevated temperatures is taken into account. As the absorption coefficient of silicon decreases exponentially with an increase in the incident wavelength, the absorption depth of visible light is much thinner than that of near infrared light (supplementary material, Fig. S1 of Part II). Based on fine structure designs, it is feasible to enhance the light absorption of a thin semiconductor absorber at shorter wavelength (solar spectrum) while limiting light absorption at longer wavelength (infrared spectrum).

The absorption coefficient (α) and the index of refraction (n) of silicon can be calculated according to the formula[30–32]

$$\alpha = \alpha_{BG} + \alpha_{FC} + \alpha_L, \tag{3}$$

$$n^2(\lambda, T) = \varepsilon(T) + \frac{L(T)}{\lambda^2}\left(A_0 + A_1 T + A_2 T^2\right), \tag{4}$$

where α_{BG}, α_{FC}, and α_L are the coefficients of the interband absorption, free-carrier absorption, and lattice-vibration absorption,[30,31] and $\varepsilon(T)$ and $L(T)$ are fitting parameters for silicon.[32] Figure 2(a) shows the measured and calculated absorptivity of a 500–μm-thick silicon wafer. The absorptivity curves of silicon wafer with different thicknesses at 1000 K are calculated as well [supplementary material, Fig. S2(a) of Part III]. One may find that, as the operating

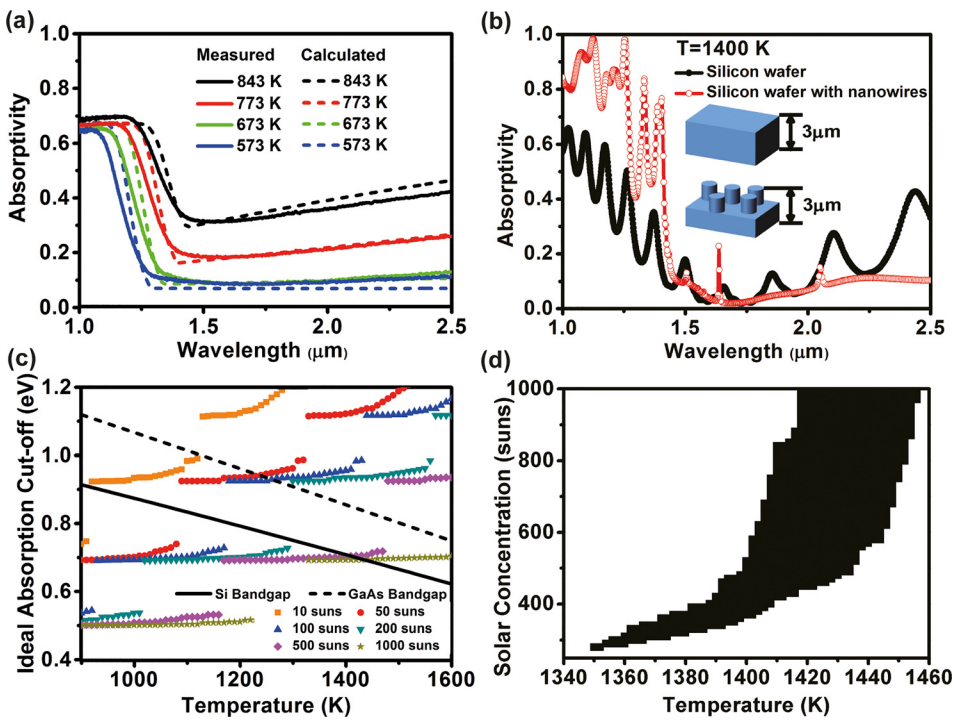

FIG. 2. (a) Measured (solid lines) and calculated (dashed lines) absorptivity of a 500-μm-thick silicon wafer at elevated temperatures. (b) Absorptivity of 3 μm silicon wafer with and without nanowires under 1400 K, both calculated by the fullwave finite difference time domain (FDTD) method. The oscillation in the absorption spectra is due to interference of the finite thickness. (c) The ideal cut-off (bandgap) of semiconductor-based SSA for different operating temperatures and solar concentrations. The dashed line refers to the bandgap of silicon (black) and gallium arsenide (gray). (d) Matching area of the bandgap of silicon and spectra intersection.

temperature increases up to 1000 K, 50 μm thick silicon absorbers can maintain a low near infrared absorptivity ($\sim$0.3). The thinner film ($\sim$3 μm) can enable such selectivity even for temperatures up to 1400 K [Fig. S2(b)]. The absorptivity spectra of a 3–μm-thick silicon wafer (under 1400 K) with and without nanowires are shown in Fig. 2(b) (see the details of optical modeling in the supplementary material, Part V 2). It is expected that because of the efficient light trapping effect of nanowire arrays, the short wavelength absorption is distinctly enhanced while the long wavelength absorption is almost unaffected.

Another unique feature of semiconductors is the temperature dependent bandgap because of thermal expansion and electron-phonon interactions. According to the Varshni empirical equation,[33] the bandgap of the semiconductor can be written as

$$E_g(T) = E_g(0) - AT^2/(B+T), \tag{5}$$

where $E_g(0)$, A, and B are the fitting parameters for different semiconductors.[34–36] Based on the parameters of silicon,[34] a red shift of bandgap $E_g(T)$ at high temperatures can be expected [Fig. 2(a)]. As the temperature increases (up to 1500 K), the silicon bandgap decreases from 1.1 eV to 0.65 eV (the ideal range for high temperature solar absorbers). The temperature dependent bandgap makes the semiconductor-based SSA quite favorable for versatile operating conditions. For solar irradiation on Earth, the maximal thermal transfer efficiency can be achieved when the spectra intersection matches the bandgap of silicon. Spectra intersection is given by

$$B(T,v) = CB_{AM1.5}(v), \tag{6}$$

where $B(T,v)$ is the Planck function spectral radiant power at temperature T and frequency v. C is the solar concentration. $B_{AM1.5}(v)$ is the solar irradiation power at frequency v with respect to the standard of AM 1.5D.

An ideal case is that the bandgap (E_g) of silicon equals the photon energy ($h\nu$) of the intersection point of the solar spectrum and blackbody irradiance, revealing the maximal efficiency condition at arbitrary temperature for SSA. Note that the solar spectrum on Earth is different from a smooth blackbody radiation curve because of absorption related to gases, dust, and aerosols.[37] These spectrum valleys will significantly change the required cut-off wavelength of the SSA[38] [Fig. 2(c)]. In other words, the spectra intersection will vary discontinuously according to the solar concentrations and operating temperatures.[12] More detailed calculations are performed from 1300 to 1500 K [Fig. 2(d)], indicating that silicon can serve as a perfect selective absorber for versatile operating conditions (temperatures of 1350–1460 K and solar concentrations of $\sim$300–1000 suns). In this area, the bandgap difference of silicon and ideal absorption cut-off is no more than 0.01 eV. Different from the selective absorbers with a fixed absorption cut-off wavelength, the temperature dependent bandgap of selective absorbers would be more convenient for system designs and implementation.

It is expected that this semiconductor-nanowire-based SSA can be applied to a wide range of material systems with different bandgaps. For example, nanowires based on gallium arsenide (GaAs) and other compound semiconductors can also be fabricated by a template assisted etching process.[39] To systematically evaluate the solar thermal efficiency of different absorbers under different operating conditions, the thermal transfer efficiency of four absorbers, including ideal blackbody, hypothetic SSA with the fixed cut-off wavelength ($\sim$1500 nm), ideal silicon, and GaAs SSA, has been calculated as a function of operating temperature as well as optical concentration (Fig. 3). In the theoretical modeling, selective

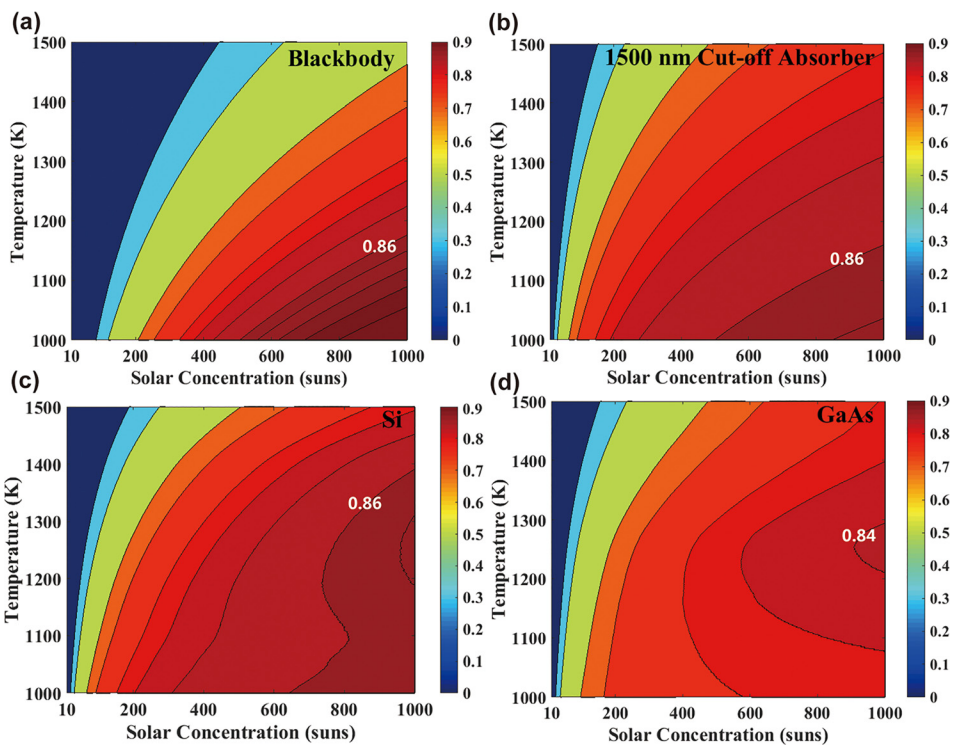

FIG. 3. Calculated thermal transfer efficiency of four different absorbers: (a) ideal blackbody, (b) a hypothetic selective absorber with a fixed cut-off wavelength of 1500 nm, (c) silicon-nanowire-based SSA, and (d) GaAs-nanowire-based SSA, respectively.

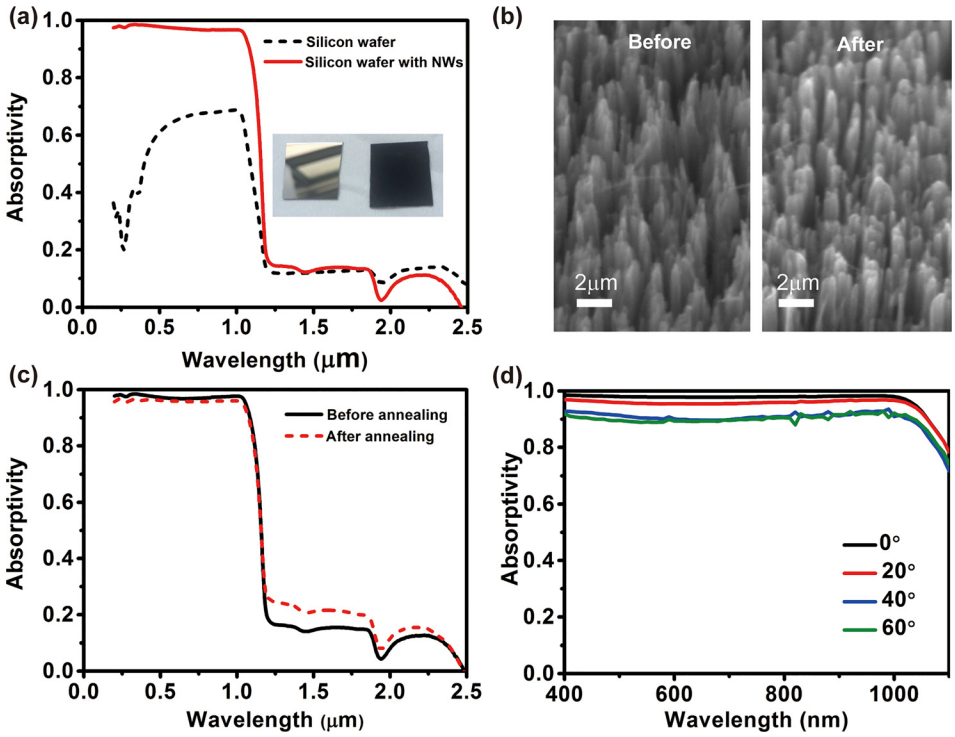

FIG. 4. (a) Measured absorptivity of black silicon (with nanowires) and silicon wafer. Insets are the optical photographs of silicon wafer (left) and black silicon with nanowires (right). (b) SEM images of silicon-nanowire-based SSA before and after annealing treatment. (c) Absorptivity of silicon-nanowire-based SSA before and after annealing treatment at 1373 K. (d) Measured absorptivity at different incident angles.

absorbers with an ideal step function absorption profile across the band edge are considered. To eliminate the influence of different values of absorptivity, the absorptivity above (below) bandgap is set as 0.97 (0.15), respectively, and W_{tran} is set as 200 nm. Particularly, GaAs has a larger bandgap than silicon and exhibits quite different temperature dependent behaviors [Fig. 2(c), gray dashed line].[35] One may find that all the SSA show higher thermal transfer efficiency than blackbody at lower solar concentrations and higher temperatures [with respect to the upper left region in Figs. 3(a)–3(d), respectively] because of more suppressed thermal emission, while the ideal blackbody would enable higher efficiency than SSA at higher solar concentrations and lower operating temperatures [with respect to the lower right region in Figs. 3(a)–3(d), respectively], as infrared emission is relatively low and solar absorption is most critical under these conditions. In addition, both silicon- and GaAs-nanowire-based SSA would perform even better than SSA with fixed cut-off wavelength under higher temperature conditions because of the temperature tunable bandgap properties.

Finally, silicon nanowires are fabricated by a scalable acid-etching process[40,41] to experimentally demonstrate the semiconductor nanowire based SSA. The black appearance of the wafer [inset in Fig. 4(a)] after the treatment indicates the desirable antireflection and light trapping properties of the random nanowires.[42–44] Therefore, it is expected that silicon nanowires can enable sharp absorption cut-off nearby the band edge. In Fig. 4(a), the sample with silicon nanowires shows absorptivity more than 97% in the range of 200–1000 nm, a 30% improvement compared to the bulk silicon wafer without any treatment. Meanwhile, there is no enhancement below the bandgap of silicon, leading to the desirable sharp cut-off with absorption decreasing rapidly from 0.97 to 0.15 across a narrow wavelength interval (W_{tran} = 200 nm). This significant enhancement can be attributed to the cone-like composite structure formed by nanowires collapse [Fig. 4(b), left].

As SSA are commonly expected to work at high temperature, thermal stability needs to be carefully examined. The silicon nanowire arrays are annealed at 1373 K for 1 h. As shown in Fig. 4(b), there is no change of morphology before and after annealing treatment. The absorption spectra before and after high temperature annealing are almost unchanged as well [Fig. 4(c)], except for a slight absorption increase (0.05) below bandgap related to the activated impurities originally existing in the sample.[30,45] The absorption performance of the nanowire-based SSA is nearly angular insensitive [Fig. 4(d)], which is beneficial for real working conditions.

In summary, we report the semiconductor-nanowire-based SSA with excellent selectivity (absorptivity above/below bandgap ~0.97/0.15) as well as extremely sharp absorption cut-off (transition bandwidth ~200 nm). In addition, the proposed SSA enable tunable absorption cut-off taking advantage of the temperature dependent bandgap of semiconductors. The thermal stability and thermal transfer efficiency under different operation conditions (temperature and solar concentration) have been systematically investigated as well, indicating superior high temperature selectivity performance. This semiconductor-nanowire-based SSA can be considered as a promising candidate for high efficiency solar thermal conversion, especially beneficial for operating conditions of high solar concentration and high temperature.

See supplementary material for the comparison of state-of-art selective absorbers, fabrication of thin silicon absorbers, model of semiconductor's absorption, and thermal transfer efficiency.

We acknowledge the micro-fabrication center of National Laboratory of Solid State Microstructures

(NLSSM) for technique support. This work was jointly supported by the State Key Program for the Basic Research of China (No. 2015CB659300), the National Natural Science Foundation of China (Nos. 11621091 and 11574143), the Natural Science Foundation of Jiangsu Province (Nos. BK20150056 and BK20151079), the Project Funded by the Priority Academic Program Development of Jiangsu Higher Education Institutions (PAPD), and the Fundamental Research Funds for the Central Universities.

[1]M. Romero and A. Steinfeld, Energy Environ. Sci. **5**, 9234 (2012).
[2]L. Zhou, Y. Tan, J. Wang, W. Xu, Y. Yuan, W. Cai, S. Zhu, and J. Zhu, Nat. Photonics **10**, 393 (2016).
[3]A. Steinfeld, Sol. Energy **78**, 603 (2005).
[4]N. Wang, L. Han, H. C. He, N. H. Park, and K. Koumoto, Energy Environ. Sci. **4**, 3676 (2011).
[5]A. Lenert, D. M. Bierman, Y. Nam, W. R. Chan, I. Celanovic, M. Soljacic, and E. N. Wang, Nat. Nanotechnol. **9**, 126 (2014).
[6]P. Bermel, M. Ghebrebrhan, W. Chan, Y. X. Yeng, M. Araghchini, R. Hamam, C. H. Marton, K. F. Jensen, M. Soljacic, J. D. Joannopoulos *et al.*, Opt. Express **18**, A314 (2010).
[7]D. Kraemer, B. Poudel, H. P. Feng, J. C. Caylor, B. Yu, X. Yan, Y. Ma, X. Wang, D. Wang, A. Muto *et al.*, Nat. Mater. **10**, 532 (2011).
[8]S. Chu and A. Majumdar, Nature **488**, 294 (2012).
[9]L. Zhou, S. Zhuang, C. He, Y. Tan, Z. Wang, and J. Zhu, Nano Energy **32**, 195 (2017).
[10]G. Ni, G. Li, S. V. Boriskina, H. Li, W. Yang, T. Zhang, and G. Chen, Nat. Energy **1**, 16126 (2016).
[11]F. Cao, D. Kraemer, T. Y. Sun, Y. C. Lan, G. Chen, and Z. F. Ren, Adv. Energy Mater. **5**, 1401042 (2015).
[12]F. Cao, K. McEnaney, G. Chen, and Z. F. Ren, Energy Environ. Sci. **7**, 1615 (2014).
[13]F. Cao, D. Kraemer, L. Tang, Y. Li, A. P. Litvinchuk, J. M. Bao, G. Chen, and Z. F. Ren, Energy Environ. Sci. **8**, 3040 (2015).
[14]J. A. Thornton and J. L. Lamb, Thin Solid Films **96**, 175 (1982).
[15]J. I. Gittleman, E. K. Sichel, H. W. Lehmann, and R. Widmer, Appl. Phys. Lett. **35**, 742 (1979).
[16]J. Moon, D. Lu, B. VanSaders, T. K. Kim, S. D. Kong, S. H. Jin, R. K. Chen, and Z. W. Liu, Nano Energy **8**, 238 (2014).
[17]J. Moon, T. K. Kim, B. VanSaders, C. Choi, Z. W. Liu, S. H. Jin, and R. K. Chen, Sol. Energy Mater. Sol. Cells **134**, 417 (2015).
[18]Y. Yin, Y. Pan, L. X. Hang, D. R. McKenzie, and M. M. M. Bilek, Thin Solid Films **517**, 1601 (2009).
[19]N. Selvakumar and H. C. Barshilia, Sol. Energy Mater. Sol. Cells **98**, 1 (2012).
[20]A. Kohiyama, M. Shimizu, and H. Yugami, Appl. Phys. Express **9**, 112302 (2016).
[21]X. F. Li, Y. R. Chen, J. Miao, P. Zhou, Y. X. Zheng, L. Y. Chen, and Y. P. Lee, Opt. Express **15**, 1907 (2007).
[22]E. Rephaeli and S. H. Fan, Opt. Express **17**, 15145 (2009).
[23]V. Rinnerbauer, A. Lenert, D. M. Bierman, Y. X. Yeng, W. R. Chan, R. D. Geil, J. J. Senkevich, J. D. Joannopoulos, E. N. Wang, M. Soljacic *et al.*, Adv. Energy Mater. **4**, 1400334 (2014).
[24]P. Li, B. Liu, Y. Ni, K. K. Liew, J. Sze, S. Chen, and S. Shen, Adv. Mater. **27**, 4585 (2015).
[25]C. E. Kennedy, *Review of Mid-to High-Temperature Solar Selective Absorber Materials* (National Renewable Energy Laboratory, Golden, Colorado, 2002).
[26]V. Rinnerbauer, S. Ndao, Y. X. Yeng, W. R. Chan, J. J. Senkevich, J. D. Joannopoulos, M. Soljacic, and I. Celanovic, Energy Environ. Sci. **5**, 8815 (2012).
[27]A. Mavrokefalos, S. E. Han, S. Yerci, M. S. Branham, and G. Chen, Nano Lett. **12**, 2792 (2012).
[28]E. Garnett and P. D. Yang, Nano Lett. **10**, 1082 (2010).
[29]J. Zhu, C. M. Hsu, Z. Yu, S. Fan, and Y. Cui, Nano Lett. **10**, 1979 (2010).
[30]H. Rogne, P. J. Timans, and H. Ahmed, Appl. Phys. Lett. **69**, 2190 (1996).
[31]P. J. Timans, J. Appl. Phys. **74**, 6353 (1993).
[32]H. H. Li, J. Chem. Phys. Ref. Data **9**, 561 (1980).
[33]Y. P. Varshni, Physica **34**, 149 (1967).
[34]V. Alex, S. Finkbeiner, and J. Weber, J. Appl. Phys. **79**, 6943 (1996).
[35]I. Vurgaftman, J. R. Meyer, and L. R. Ram-Mohan, J. Appl. Phys. **89**, 5815 (2001).
[36]J. S. Blakemore, J. Appl. Phys. **53**, R123 (1982).
[37]M. P. Thekaekara, *The Solar Constant and the Solar Spectrum Measured from a Research Aircraft* (NASA, Washington, 1970).
[38]A. Lenert, Y. Nam, D. M. Bierman, and E. N. Wang, Opt. Express **22**, A1604 (2014).
[39]G. Mariani, R. B. Laghumavarapu, B. T. de Villers, J. Shapiro, P. Senanayake, A. Lin, B. J. Schwartz, and D. L. Huffaker, Appl. Phys. Lett. **97**, 013107 (2010).
[40]K. Q. Peng, J. J. Hu, Y. J. Yan, Y. Wu, H. Fang, Y. Xu, S. T. Lee, and J. Zhu, Adv. Funct. Mater. **16**, 387 (2006).
[41]K. Q. Peng, Y. J. Yan, S. P. Gao, and J. Zhu, Adv. Funct. Mater. **13**, 127 (2003).
[42]K. Q. Peng and S. T. Lee, Adv. Mater. **23**, 198 (2011).
[43]M. Steglich, D. Lehr, S. Ratzsch, T. Kasebier, F. Schrempel, E. B. Kley, and A. Tunnermann, Laser Photonics Rev. **8**, L13 (2014).
[44]L. Hu and G. Chen, Nano Lett. **7**, 3249 (2007).
[45]S. M. Sze and J. C. Irvin, Solid State Electron. **11**, 599 (1968).